

pubs.acs.org/Macromolecules Article

Superionic Li-Ion Transport in a Single-Ion Conducting Polymer Blend Electrolyte

Benjamin A. Paren, Nam Nguyen, Valerie Ballance, Daniel T. Hallinan, Justin G. Kennemur, and Karen I. Winey*



Cite This: *Macromolecules* 2022, 55, 4692–4702



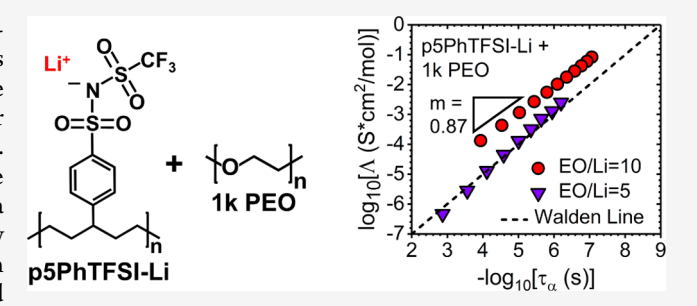
ACCESS I

Metrics & More

Article Recommendations

s Supporting Information

ABSTRACT: Single-ion conducting polymers (SICs) are promising candidates for the next generation of safer polymer electrolytes due to their stability and high transference number. However, the conductivity in SICs is often limited by the mobility of the polymer backbone as the ion mobility is coupled to segmental relaxations. We present polymer blend electrolytes, consisting of a precise single Li-ion conducting polymer with a (trifluoromethanesulfonyl)imide anion pendant group and a low molar mass poly(ethylene oxide) (PEO). Dielectric relaxation spectroscopy is used to probe both the ion transport properties and segmental dynamics of these blends, and X-ray scattering is used to



evaluate their morphology. PEO associates with the ionic groups of the SIC, forming a miscible blend with pathways that promote ion transport. At a high PEO content (an ethylene oxide to Li⁺ ratio of 10), ionic conductivities greater than 10⁻⁵ and 10⁻⁴ S cm⁻¹ are achieved at 90 and 130 °C, respectively. A comparison of conductivities and polymer relaxation times shows that the high PEO content blends exhibit superionic transport, in which there is some decoupling of the Li-ion motion from the backbone mobility. This superionic transport is uncommon in single Li-ion conductors above the glass transition temperature, thus this work presents a critical step toward establishing design rules for superionic transport in SICs.

INTRODUCTION

There is major interest in developing advanced lithium-ion batteries due to their high energy densities compared to other energy storage technologies.^{1,2} Currently, conventional liquid electrolytes still dominate the lithium-ion battery market because of their superior ionic conductivity. However, liquid electrolytes typically have multiple disadvantages including electrochemical instability, volatility, flammability, and dendrite formation.³ Solid polymer electrolytes (SPEs) have been extensively investigated as an alternative, with improved safety, flame resistance, and compatibility with high specific energy electrode materials. SPEs are generally composed of a lithium salt that is mixed with a solvating polymer to promote ion dissociation. Of those that have been studied, poly(ethylene oxide) (PEO) still remains the most popular solvating polymer due to its ubiquity, low glass transition temperature (T_g) , and ability to solvate lithium ions through chelation. 4-6 As the archetypal design of SPE is classified as the dual-ion conductor, the diffusion of both the cation and anion can lead to similar hurdles that liquid electrolytes must overcome.

Single-ion conductors (SICs) are a class of SPEs in which one of the ionic species (often the anion) is covalently bonded to the polymer. SICs are either synthesized through polymerization of functionalized monomers or post-polymerization modification. The mobility of the covalently bound anions is

limited during battery cycling, which can lead to a high transference number for Li⁺ and can prevent the concentration gradients that typically cause voltage losses and reduction in performance. Although significant efforts have been focused on PEO-based SICs, the majority of PEO-based SICs exhibit ionic conductivities of 10⁻⁵ to 10⁻⁴ S cm⁻¹ at 90 °C, ^{2,8,9} which are still below the desired ionic conductivities for commercialization (above 10⁻³ S cm⁻¹ at room temperature). Achieving superior ionic conductivity in PEO-based SICs is limited by the high degree of crystallinity of PEO at room temperature as well as the regulated ion transport that depends on segmental mobility. Above the $T_{\rm g}$ of the SICs, ion transport is dominated by segmental mobility of polymer chains, in which they exhibit a Vogel–Fulcher–Tammann (VFT) conductivity dependence on temperature. $^{10-12}$ Ion transport in SICs in the glassy state, on the other hand, has been shown to be dominated by transport decoupled from the segmental dynamics of polymer backbones that exhibit Arrhenius dependence on temper-

Received: March 4, 2022 Revised: April 30, 2022 Published: May 25, 2022





Figure 1. Synopsis of the synthesis route to p5PhTFSI-Li, adapted from Nguyen et al., in which the synthesis is reported elsewhere. 33

ature. 10,13,14 The ionic conductivities in this Arrhenius regime, however, are often several orders of magnitude lower than those of liquid electrolytes or SICs above the $T_{\rm g}$.

A key limitation in polymer electrolytes is that ion conductivity is typically strongly coupled to the mobility of the polymer backbone, which can prevent the high conductivities of liquid electrolytes from being achieved. To address this, some recent studies have focused on decoupling ion transport from the polymer backbone, particularly in SICs. When comparing molar conductivity with segmental relaxation time, conductivities that fall above the "ideal" Walden line are considered to be superionic, with at least some degree of decoupling of ionic transport from segmental relaxation time. 15,16 Decoupled transport is most common below the T_{g} , but is challenging to access far above the T_{g} , or in the melt state, when conductivity begins to approach target values of $\sim 10^{-3}$ S cm⁻¹. While this superionic transport has been reported for some salt-in-polymer electrolytes, as well as polymerized ionic liquids, we believe it has not previously been reported above the T_g for a single Li-ion conductor. ^{15–18} Our recent work has utilized experiments and atomistic molecular dynamics (MD) simulations to demonstrate the potential for cations to move along percolated ionic assemblies, faster than the segmental dynamics of the polymer backbone. 19,20 Others have also theorized that the formation of nanochannels from percolated ionic aggregates can assist ion transport, with ion correlations that result in enhanced charge delocalization and reduced activation energy. 21,22 Therefore, establishing percolating aggregate networks in SICs is desired to maximize ion mobility faster than the polymer backbone. We recently reported decoupled cation transport through percolated aggregates in precise polyethylenes with cation-neutralized phenyl sulfonate pendant groups on every fifth backbone carbon below the $T_{\rm g}$. These ionomers were synthesized from ring-opening metathesis polymerization (ROMP) of 4-phenylcyclopentene monomers, followed by hydrogenation and sulfonation of the phenyl moieties.^{23,24} The ionic conductivity of the Li-neutralized polymer is on the order of 10^{-7} S cm⁻¹ at 180 °C $(T_g > 220^{\circ})$, which is still several orders of magnitude below the values that liquid electrolytes can provide, so more must be done to improve ion-percolated systems such as this.

To further improve the ionic conductivity in SICs, factors that need consideration are the polyanion size and charge-delocalization because they affect dissociation of ions, as well as the mobility of the polymer. Generally, bulkier and more charge-delocalized ions are preferred to improve ion dissociation in polymer electrolytes. MD simulations also suggest that decoupled ion transport can be enhanced by increasing the size of the bound ion in the polymers. A frequently studied lithium salt in SPEs is lithium bis-(trifluoromethanesulfonyl) imide (LiTFSI) due to its bulkiness

and high charge delocalization. 26-28 The TFSI- counteranions were first incorporated to polymer chains by Meziane et al.²⁹ to obtain TFSI-based SICs from the derivatization of a styrenic monomer and were adapted in various forms of polymer backbones to investigate the effect on different properties. 29-32 TFSI-functionalized SICs, with polystyrene-based backbones (PSTFSI-Li) and poly(acrylic acid)-based backbones (PATF-SI-Li), have also been blended with PEO to improve ion transport, achieving conductivities of ~10⁻⁵ S cm⁻¹ at 80 °C. ^{29,31} However, to further increase conductivity in SICs, it is critical to understand the underlying mechanisms behind the transport phenomena and determine ways to achieve superionic transport above the $T_{\rm g}$. This study focuses on recently synthesized pSPhTFSI–Li, a precise polyethylene with a LiTFSI-functionalized phenyl group spaced every five carbons along the backbone (Figure 1). The synthesis of p5PhTFSI-Li is reported in Nguyen et al., which also includes work done in parallel with this study that describes some of the electrochemical characterization of the neat p5PhTFSI-Li and blends with 20,000 g mol⁻¹ PEO.³³ The parallel study found that p5PhTFSI-Li blended with 20,000 g mol⁻¹ PEO exhibited a Li+ transference number of approximately 1 and a conductivity of $\sim 10^{-4}$ S cm⁻¹ at 90 °C at certain blend ratios, which are promising for an application as a SPE. In this study, we blend p5PhTFSI-Li with low-molecular-weight PEO (1000 g mol-1) and, for the first time, characterize the nanoscale structure and polymer dynamics in combination with the ion transport properties. In blends with a ratio of ethylene oxide to Li+ (EO/Li) of 10, we determine that the system exhibits superionic transport well above the T_{φ} which is uncommon in single Li-ion conducting polymers.

■ MATERIALS AND EXPERIMENTAL METHODS

Materials and Sample Preparation. p5PhTFSI—Li was made starting from poly(4-phenylcyclopentene) (P4PCP), which is produced through ROMP and features a precise linear polyethylene backbone with an atactic phenyl branch on every fifth carbon following mild hydrogenation of the olefins (p5Ph). 24 The synthesis of p5PhSA-Na was then adapted from Kendrick et al., and the degree of sulfonation is 94%. 23,24 The number average degree of polymerization $(N_{\rm n})$ is 89, and the dispersity (D) is $\sim\!1.6$. The synthesis of p5PhTFSI—Li from p5PhSA-Na is shown in Figure 1. From the calculations first presented in Nguyen et al., it was determined that 90% of the phenyl groups were successfully functionalized with a TFSI—Li moiety. In other words, the conversion efficiency from SA—Na to TFSI moieties was 96%. 33 The detailed synthesis and characterization of these materials, including thermal gravimetric analysis (TGA), size exclusion chromatography (SEC), and multinuclear magnetic resonance (1 H, 13 C, and 19 F NMR), are reported in a work conducted parallel to this study. 33

PEO with a methyl ether at both ends and a number average molar mass $(M_{\rm n})$ of $\sim 1000~{\rm g~mol}^{-1}~(N_{\rm n}=22)$ was obtained from Millipore Sigma (product no. 445894). Appropriate amounts of lyophilized pSPhTFSI–Li and as-received PEO were mixed to obtain the

following ethylene oxide to Li⁺ (EO/Li) ratios: 0, 2, 5, and 10. These polymer mixtures were dissolved in deionized water (2–3 wt % polymer in solution) and stirred for at least 1 h at 23 \pm 2 °C. Solutions were then drop cast onto 100 μm teflon at 80 °C, and the solvent was evaporated to form polymer blend films. The as-cast polymer films were dried at high temperature under vacuum, as detailed below, before each of the measurements: differential scanning calorimetry (DSC), X-ray scattering, and dielectric relaxation spectroscopy (DRS).

Thermal Characterization. DSC was performed on the p5PhTFSI–Li blends and the neat PEO. The as-cast polymer films (4-10 mg) were dried at $180 \,^{\circ}\text{C}$ for 1-2 days (EO/Li = 0 and 2) and $120 \,^{\circ}\text{C}$ for >12 h (EO/Li = 5 and 10, and neat PEO) under vacuum, then immediately sealed in DSC pans for testing using a TA instruments QA 1000 differential scanning calorimeter. Samples went through at least two cooling and heating cycles, at $10 \,^{\circ}\text{C/min}$, with all samples heated to at least $150 \,^{\circ}\text{C}$ and cooled to as low as $-140 \,^{\circ}\text{C}$ depending on the PEO content. The final heating was used to determine the T_g values and the melting point (neat PEO only).

X-ray Scattering. X-ray scattering measurements were performed at room temperature on the p5PhTFSI-Li blends and neat PEO. The as-cast polymer films (100-200 μ m thick) were dried at 180 °C for 1-2 days (EO/Li = 0 and 2) and at 120 °C for >12 h (EO/Li = 5 and 10, and neat PEO) immediately before structural characterization. The dual source and environmental X-ray scattering facility operated by the Laboratory for Research on the Structure of Matter at the University of Pennsylvania, with a Xeuss 2.0 system (Xenocs) and a GeniX3D Cu source ($\lambda = 1.54$ Å), was used for X-ray scattering measurements. Sample-to-detector distances for X-ray scattering were 35 cm for small angles (SAXS) and 16 cm for wide angles (WAXS), covering a total q range of 0.05–2.0 Å⁻¹. Samples were mounted on a mica window and measured for at least 1 h. The 2D X-ray scattering profiles are isotropic and thus were azimuthally integrated to 1D data using Foxtrot software after subtracting the mica window background. X-ray scattering peak positions were determined using the simultaneous fitting of scattering peaks with pseudo-Voigt functions as shown in Figure S1. The neat PEO and EO/Li = 10 samples were also measured at higher temperatures using a Linkam HFSX350-GI stage. PEO was measured at 60 °C in order to obtain a scattering profile above its melting point. p5PhTFSI-Li EO/Li = 10 was measured at select temperatures upon cooling from 130 to 30 °C, keeping at each temperature for 1 h.

Dielectric Relaxation Spectroscopy. Ionic conductivity and dielectric relaxations were determined using DRS. The as-cast p5PhTFSI-Li blend films (50-100 µm thick) were sandwiched between two stainless steel electrodes, with silica spacers. The polymer-electrode assembly was placed into a cryostat and equilibrated under vacuum at 180 °C for 1-2 days (EO/Li = 0 and 2) and at 120 °C for >12 h (EO/Li = 5 and 10) to ensure any remaining water was removed and to maximize wetting of the polymer with the electrode interface. The measurements were performed using a Solartron Modulab XM materials test system in the frequency window 10^{-1} – 10^6 Hz under an applied voltage of 0.5 V. The polymers were measured every 5 °C upon cooling and held for 20 min at each temperature before measurement to let the polymer equilibrate. In addition, polymers were measured upon heating to ensure reversibility. The polymers remained in a constant vacuum environment during the entirety of their equilibration and measurement. Temperature ranges varied per sample and included all of the temperatures at which a DC conductivity feature appeared in the frequency window of $10^{-1}-10^6$ Hz. The temperature ranges were $120-190 \, ^{\circ}\text{C} \, (EO/\text{Li} = 0), \, 90-180 \, ^{\circ}\text{C} \, (EO/\text{Li} = 2), \, 40-140 \, ^{\circ}\text{C}$ (EO/Li = 5), and 30–130 °C (EO/Li = 10). Impedance data (Z' vs -Z'') were fit with an equivalent circuit model to determine the through-plane high-frequency resistance R, which is used to calculate the through-plane conductivity, $\sigma_{DC} = L/AR$, where L is the film thickness and A is the cross-sectional area (determined using ImageJ software area analysis), Figure S2. The permittivity spectra (ε' and ε'') were also used to calculate conductivity and dielectric relaxation information as detailed below.

RESULTS AND DISCUSSION

Thermal Properties of Blends. DSC was employed to investigate the $T_{\rm g}$ as well as PEO crystallinity in the blends of pSPhTFSI—Li and PEO, and will be further corroborated with ionic conductivity and X-ray scattering results in later sections. DSC thermograms of the neat polymers and different blend compositions of PEO and pSPhTFSI—Li are shown in Figure 2a. An endothermic transition was observed in 1000 g mol⁻¹

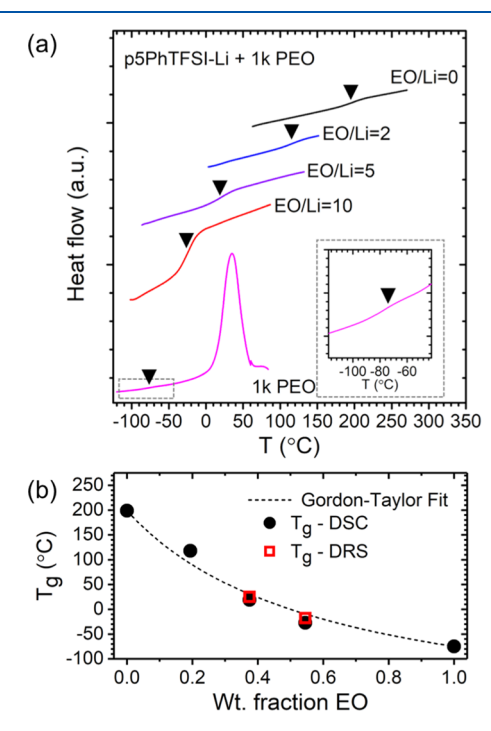


Figure 2. (a) DSC thermograms of heating of pSPhTFSI–Li, PEO, and their blends. Inverse triangles denote $T_{\rm g}$ values at the midpoint. (b) Corresponding $T_{\rm g}$ for different PEO contents and fitting with eq 1 (k=0.38). $T_{\rm g}$ values determined from DRS analysis of EO/Li = 5 and 10 (detailed later) are also included.

PEO at 30 °C upon heating, and this is attributed to the melting of PEO crystallinity into an amorphous state. PEO has a crystallinity 34 of 69%. PEO also exhibits a $T_{\rm g}$ of -75 °C, consistent with PEO of low $M_{\rm n}$. Neat pSPhTFSI—Li exhibits a single $T_{\rm g}$ 199 °C, which is higher than that of the parent pSPh $(T_{\rm g}=17~{\rm ^{\circ}C}),^{24}$ as a result of bulkier side groups and interactions between ionic groups. This is lower than previously reported $T_{\rm g}$ for the polystyrene-based SIC, PSTFSI—Li (212–256 °C), 10,11,35 likely due to the more flexible nature of the pSPh backbone compared to PS and the lower overall ion content. Upon addition of PEO into pSPhTFSI—Li, there is a significant reduction in $T_{\rm g}$, and all blends exhibit only a single $T_{\rm g}$ which indicates a miscible polymer blend. 15,36,37 The absence of a melting peak in any of the blends also suggests a single-phase system and suggests that ion transport in these blends will not be impeded by a crystalline PEO phase.

The T_g values fit well (Figure 2b) with the Gordon-Taylor equation 38

$$T_{\rm g} = \frac{W_1 T_{\rm g,1} + k W_2 T_{\rm g,2}}{W_1 + k W_2} \tag{1}$$

where W_1 and W_2 are the weight fractions of each homopolymer component, PEO and p5PhTFSI-Li, respectively, and $T_{\rm g,1}$ and $T_{\rm g,2}$ are the $T_{\rm g}$ values of neat PEO and p5PhTFSI-Li, respectively. The parameter k accounts for the deviation from ideal mixing of binary mixtures and unequal contribution of each homopolymer component into the resulting T_g . For the p5PhTFSI-Li/PEO blends, a value of k= 0.38 results in the best fitting of the Gordon-Taylor model and is similar to k reported for other single Li-ion conductors blended with PEO. 39,40 While a single $T_{\rm g}$ indicates a singlephase material, k < 1 suggests that the local dynamics are dominated by specific local interactions. In p5PhTFSI-Li blends, this is consistent with strong interactions between the TFSI-Li groups and the ether oxygen in PEO, and weaker interactions between the nonpolar p5Ph backbone and PEO. The T_g values of the EO/Li = 5 and 10 blends were also obtained from an analysis of segmental relaxation from the DRS measurements, as detailed in the following sections, with good agreement.

Nanoscale Morphology. X-ray scattering was performed on the pSPhTFSI-Li/PEO blends at 25 °C (Figure 3), and all

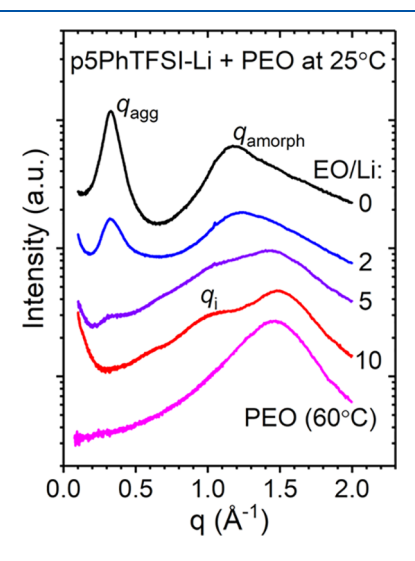


Figure 3. X-ray scattering data of neat pSPhTFSI–Li and blend compositions of pSPhTFSI–Li with PEO ($M_{\rm n}=1000~{\rm g~mol}^{-1}$) at 25 °C, shifted vertically for clarity. For comparison, the data were plotted against X-ray scattering data of neat PEO at 60 °C. The X-ray profile of PEO at 25 °C can be found in the Supporting Information (Figure S3).

of the blends exhibit an asymmetric amorphous halo. For neat p5PhTFSI, the maximum of this amorphous halo is $q_{\rm amorph} \sim 1.2~{\rm Å}^{-1}$. This peak shifts toward the position of melt-state PEO in the EO/Li = 10 blend, $q_{\rm amorph} \sim 1.4~{\rm Å}^{-1}$, which is comparable to that of the amorphous halo found in PEO at 60 °C. The PEO (1000 g mol⁻¹) is semicrystalline at 25 °C, showing multiple sharp peaks in the range $q=1-2~{\rm Å}^{-1}$ (Figure S3). The absence of crystalline peaks in Figure 3 represents purely amorphous blends, indicating the miscibility between 1000 g mol⁻¹ PEO and p5PhTFSI–Li. If the polymers were phase-separated, it is likely that some of the PEO would crystallize, which is not evident in the room-temperature X-ray scattering or DSC results.

In addition to the amorphous halo, neat p5PhTFSI-Li exhibits q_{agg} at 0.33 Å⁻¹, which is associated with the characteristic length scale $d_{agg} = 19$ Å of the ionic aggregates (Figure 4), where $d = 2\pi/q$. In the previous study of p5PhSA— Li, which combined X-ray scattering and atomistic MD simulations, d_{agg} corresponds to the center-to-center spacing between distinct sections of a percolated aggregate. Thus, we assign the low-angle peak found in the p5PhTFSI-Li and the blends to the ionic aggregates. This spacing is a primary factor determining the aggregate spacing. 19 Upon addition of PEO to pSPhTFSI-Li, the intensity of the q_{agg} peak decreases while maintaining a similar position in the EO/Li = 2 and 5 blends, with $d_{\text{agg}} \sim 19$ Å (Table S1), and this aggregate peak disappears in the EO/Li=10 blend. Previous studies of PEObased copolymer ionomers have also demonstrated the disappearance of $q_{agg'}$ which was attributed to the suppression of ionic aggregation by the addition of PEO. 41,42 However, we propose that the weakening of q_{agg} with increasing PEO content in the p5PhTFSI-Li/PEO blends is likely the result of a loss of scattering contrast between the polar and nonpolar phases. Estimates of the electron densities, based on the van der Waals volume (VDWV),⁴³ of p5Ph (~504 nm⁻³) and amorphous PEO (~488 nm⁻³) are very similar and both lower than that of TFSI-Li (835 nm⁻³), so the addition of PEO to the ionic domains reduces the electron density differences between the polar and nonpolar domains.

This phenomenon has been reported in computational and experimental studies of multiple sulfonated proton-conducting polymers swollen with water. In those studies, the presence of water lowers the electron density of the sulfonated polar domains, to values similar to that of the nonpolar backbone, leading to the disappearance of the aggregate peak, even

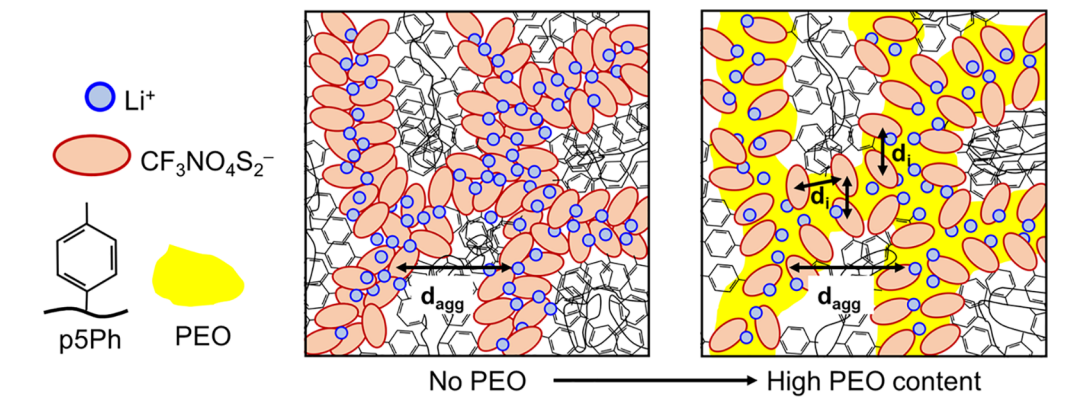


Figure 4. Illustration of expected phase behavior ranging from low to high PEO content in the p5PhTFSI-Li/PEO blends. Note that the low-molecular-weight PEO is amorphous in the blends.

though there is still nanophase separation. We suspect a similar behavior in p5PhTFSI-Li and PEO blends, where 1000 g mol⁻¹ PEO interacts with the ions to swell the polar domains, decreasing the electron density of the ions and reducing the overall electron density contrast in the blends as a function of PEO content. Figure 4 schematically shows the nanoscale morphology without and with PEO swelling the ionic assemblies and maintain d_{agg} . The interaction of the PEO with the ions is further demonstrated at the high PEO contents of EO/Li = 5 and EO/Li = 10, with an additional peak, q_i , that appears at $\sim 1 \text{ Å}^{-1}$, or $d_i \sim 6 \text{ Å}$, Figure 4. This peak corresponds to scattering from anion-anion correlations, and has been frequently reported in studies of polymerized ionic liquids. 46-48 Recent work by Balsara and co-workers reported a similar $d_i = 7$ Å in blends of PEO with LiTFSI salt, further indicating that d_i is approximately the anion—anion distance in our p5PhTFSI-Li blends. 49 To explore the behavior of the q_i peak with temperature, we selected one system exhibiting this peak, EO/Li = 10, and performed X-ray scattering at select temperatures on cooling (130, 110, 90, and 50 °C), Figure S4. Overall, the scattering results are similar indicating continued blend miscibility. Figure 5 illustrates the change in d_{amorph} and

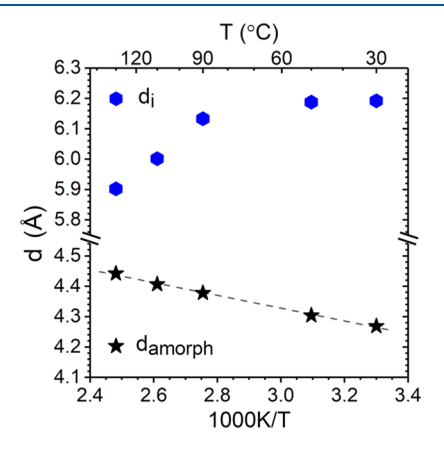


Figure 5. d_i and d_{amorph} of the p5PhTFSI-Li/PEO EO/Li = 10 blend as a function of temperature. Results obtained from fits of data in Figure S4. The dashed line is a linear fit through d_{amorph} .

 $d_{\rm i}$ with temperature for the EO/Li = 10 blend. $d_{\rm amorph}$ decreases linearly as T^{-1} increases, which is consistent with thermal expansion of a polymer above the $T_{\rm g}$. Conversely, $d_{\rm i}$ increases with T^{-1} , suggesting ions are closer together at a higher temperature with $d_{\rm i}$ = 5.9 at 130 °C. Previously studied PEO-based sulfonate copolymers have shown aggregation to occur upon heating, a result of stronger columbic interactions between ions occurring at higher temperatures. 50 Here, the ions remain solvated by the PEO, and the reduced interion distance may similarly be a result of stronger columbic interactions at higher temperatures.

While we did not observe phase separation in these blends with 1000 g mol⁻¹ PEO, higher PEO concentrations could induce macrophase separation. In the parallel study on p5PhTFSI–Li blended with 20,000 g mol⁻¹ PEO, it was reported that at high PEO contents (>70 wt % PEO), there is evidence of macrophase separation.³³ This suggests that as we increase the PEO content in these 1000 g mol⁻¹ PEO blends, even before macrophase separation occurs, the LiTFSI functional groups may begin to expel excess PEO toward the center of the polar domains. At a sufficiently high PEO content, this could lead to macrophase separation, as seen in the 20,000 g mol⁻¹ blends.³³

Ionic Conductivity. Ionic conductivity (σ_{DC}) of pSPhTFSI–Li with varying PEO contents was examined as a function of temperature, Figure 6a. σ_{DC} was determined from the Nyquist plot by fitting to an equivalent circuit model (Figure S2), and is completely reversible for all of the blends studied upon heating and cooling (Figure S5). Neat pSPhTFSI–Li exhibits Arrhenius behavior (fitting parameters in Table S2) and has ionic conductivity from 10^{-11} S cm⁻¹ at 120 °C to 10^{-8} S cm⁻¹ at the highest measured temperature of 190 °C.

$$\sigma_{\rm DC} = \sigma_0 \, \exp\!\left(\frac{-E_{\rm a}}{RT}\right) \tag{2}$$

The activation energy of ~130 kJ mol⁻¹ and values of conductivity are very similar to those of previously reported functionalized polystyrenes, PSTFSI–Li. ^{10,11,35} This is expected when the functional groups are the same, and decoupled ion transport occurs in a similar local environment.

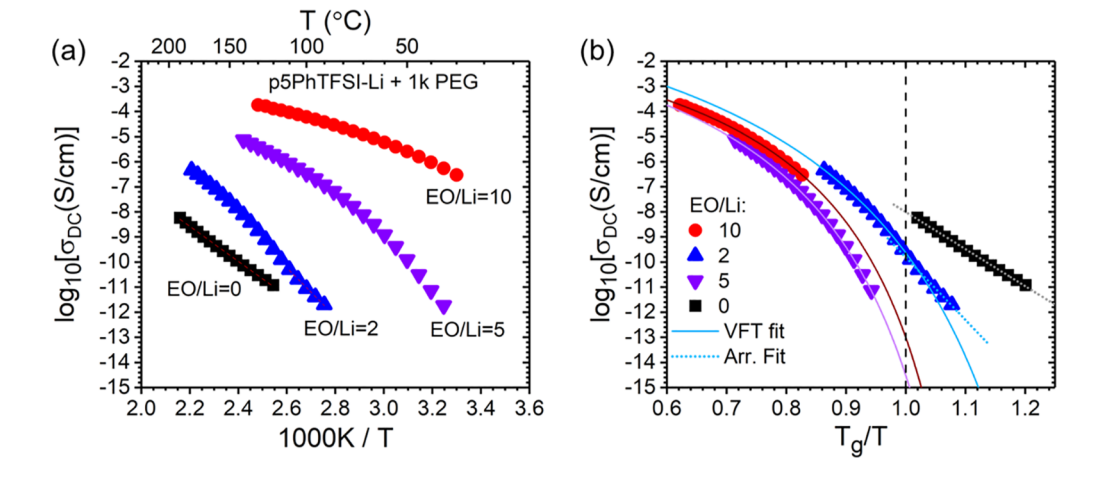


Figure 6. (a) Ionic conductivity of neat p5PhTFSI–Li and blend compositions with PEO as a function of temperature. (b) $T_{\rm g}$ -normalized ionic conductivity of neat p5PhTFSI–Li and different EO/Li concentrations along with VFT and Arrhenius fits of conductivity (eqs 2 and 3). Vertical dashed line represents $T_{\rm g}/T=1$. The $T_{\rm g}$ for EO/Li = 5 and 10 is the mean of $T_{\rm g-DSC}$ and $T_{\rm g-DRS}$, and the $T_{\rm g}$ for EO/Li = 0 and 2 is just $T_{\rm g-DSC}$ because $T_{\rm g}$ for these samples could not be determined from DRS measurements.

As PEO is added to p5PhTFSI-Li, conductivity increases significantly, with EO/Li = 10 exhibiting the fastest ion transport of all blends studied. The EO/Li = 10 blend has a $\sigma_{\rm DC}$ of 3.8 \times 10⁻⁵ S cm⁻¹ at 90 °C and 1.8 \times 10⁻⁴ S cm⁻¹ at 130 °C, which is 7 orders of magnitude greater than that of EO/Li = 0 at the same temperature. The drastic increase in conductivity is largely due to the increase in polymer mobility in the amorphous blends from the low- T_g PEO. These conductivity values are consistent with those reported for p5PhTFSI-Li blended with 20,000 g mol⁻¹ PEO in a concurrent study.³³ The EO/Li = 10 conductivity values are also similar to those measured in PSTFSI-Li/PEO blends by Meziane et al. and Ma et al. 29,51 Note that the p5PhTFSI-Li used here was synthesized using postpolymerization modification, as opposed to monomer synthesis for PSTFSI-Li, demonstrating an alternative route to access this level of ion transport.

To improve polymer electrolyte design, it is critical to understand the mechanisms of ion transport that are present. $\sigma_{\rm DC}$ exhibits VFT-like behavior (Figure 6b, fitting parameters listed in Table S2) in the EO/Li = 5 and 10 blends at all temperatures tested (at $T\gg T_{\rm g}$), thus indicating a dependence on segmental mobility in ion transport.

$$\sigma_{\rm DC} = \sigma_{\infty} \exp\left(\frac{-B}{T - T_0}\right) \tag{3}$$

For EO/Li = 2, a VFT-to-Arrhenius transition in $\sigma_{\rm DC}$ occurs at approximately its $T_{\rm g}$ of 118 °C (Figure 6b), as the dominant ion transport mechanism transitions between decoupled hopping and coupled with segmental relaxation. At $T_{\rm g}$, the conductivity is highest for neat pSPhTFSI–Li, 10^{-8} S cm $^{-1}$, which is expected due to ionic aggregates that facilitate decoupled ion transport when the polymer is glassy. The conductivity at $T_{\rm g}$ is reduced with the addition of PEO. This is because transport of Li⁺ in PEO is typically dominated by the mobility of the PEO chains. Thus, when taken below $T_{\rm g}$, Li⁺ surrounded by PEO becomes immobile compared to Li⁺ ions that are free to hop between neighboring TFSI $^-$ groups.

It is well reported that when ion dynamics are completely coupled to segmental relaxations of the polymer, $\sigma_{\rm DC}$ should be in the order of 10^{-15} to 10^{-14} S cm $^{-1}$ at the $T_{\rm g}.^{11}$ This is the case for EO/Li = 5, which has $\sigma_{\rm DC} \sim 10^{-15} - 10^{-14}$ S cm $^{-1}$ at $T_{\rm g}$. However, the VFT fit of EO/Li = 10 intersects with $T_{\rm g}/T=1$ at 10^{-13} S cm $^{-1}$, suggesting at least some amount of decoupled transport is taking place at and above the $T_{\rm g}$. We further explore the segmental dynamics and decoupling of ion transport by analyzing the dielectric permittivity spectra.

Correlating Ion Transport with Segmental Dynamics. The real (ε') and imaginary (ε'') components of the complex permittivity spectra $\varepsilon^*(\omega)$ are described by ⁵²

$$\varepsilon^*(\omega) = \varepsilon' - i\varepsilon'' \tag{4}$$

The complex permittivity was modeled (Figure 7) by the superposition of a Havriliak—Negami (HN) function and a term accounting for DC conductivity and electrode polarization 53-55

$$\varepsilon^{*}(\omega) = \varepsilon_{\infty} + \frac{\sigma_{\rm DC}}{i\omega} \frac{(i\omega\tau_{\rm EP})^{\gamma}}{[1 + (i\omega\tau_{\rm EP})^{\gamma}]} + \frac{\Delta\varepsilon_{\alpha}}{[1 + (i\omega\tau_{\rm HN-\alpha})^{a}]^{b}}$$
(5)

where ε_{∞} accounts for the permittivity at infinite frequency, the second term accounts for conductivity, $\sigma_{\rm DC}$, and electrode

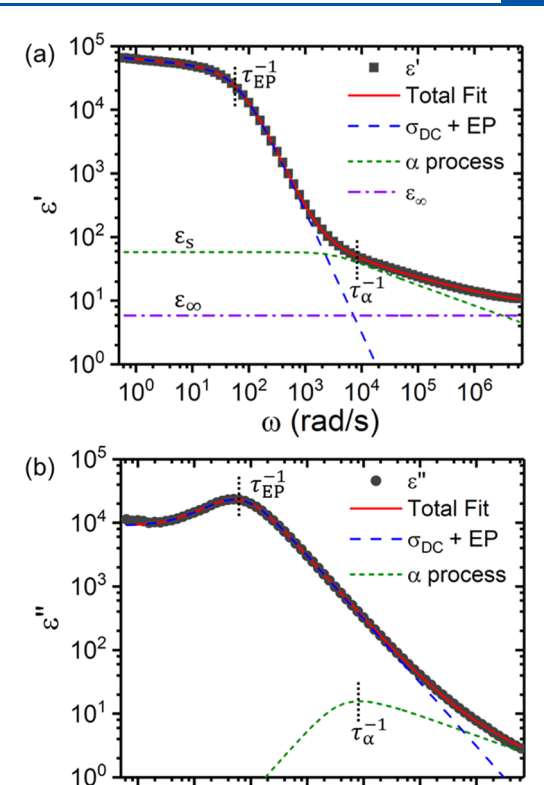


Figure 7. (a) ε' and (b) ε'' , with fits to the total and individual components of eq 5. This example is for EO/Li = 10 at 30 °C. $\varepsilon_{\rm s}$, ε_{∞} $\tau_{\rm EP}$, and τ_{α} are labeled to illustrate where along the spectra these phenomena occur.

 10^{3}

ω (rad/s)

 10^{4}

 10^{5}

 10^{2}

10¹

polarization, where $\tau_{\rm EP}$ is the relaxation time associated with electrode polarization, γ is the corresponding shape parameter for broadening of this relaxation, and the final term corresponds to a dielectric relaxation, either the α or α_2 process, where $\Delta \varepsilon_{\alpha/\alpha_2}$ is the strength of the relaxation $(\Delta \varepsilon_{\alpha/\alpha_2} = \varepsilon_s - \varepsilon_\infty)$, $S^{2,56}$ $\tau_{\rm HN-\alpha}$ is the HN relaxation time, and a and b are the shape parameters corresponding to symmetric and asymmetric broadening of the relaxation, respectively, where $0 < a \le 1$ and $0 < ab \le 1$. Equation 5 fits well to the experimental data, as is demonstrated in Figure 7. We note that the $\sigma_{\rm DC}$ values obtained by fitting with eq 5 results in the same values as from previous fitting to the equivalent circuit model, as is expected (Figure S6). We use these parameters to compute the relaxation times, τ_α and $\tau_{\alpha 2}$ with $t^{12,57}$

$$\tau_{\alpha/\alpha_2} = \tau_{\text{HN}-\alpha/\alpha_2} \left(\sin \frac{a\pi}{2+2b} \right)^{-1/a} \left(\sin \frac{ab\pi}{2+2b} \right)^{1/a} \tag{6}$$

The τ_{α} process corresponds to segmental relaxation of PEO coordinated with LiTFSI, and $\tau_{\alpha 2}$ to the rearrangement of ions. ^{12,57,58} We distinguish τ_{α} and $\tau_{\alpha 2}$ by fitting to the relaxation time form of the VFT equation

$$\tau_{\alpha} = \tau_{\infty} \exp\left(\frac{B}{T - T_0}\right) \tag{7}$$

In polymers, it is generally accepted that the glass transition occurs when the segmental relaxation time τ_{α} is ~100–1000 s. ^{12,57,58} In Figure 8a, the $T_{\rm g}$ from DRS is the temperature at

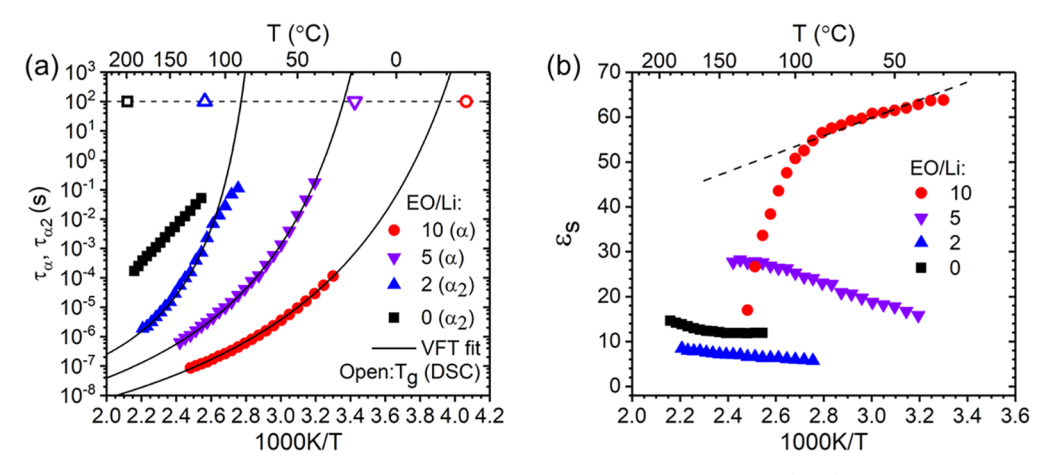


Figure 8. (a) τ_{α} and $\tau_{\alpha 2}$ vs inverse temperature for the pSPhTFSI–Li blends. Solid lines are VFT fits (eq 7), with fitting parameters listed in Table S3. The horizontal dashed line represents $\tau_{\alpha/\alpha 2} = 100$ s, and the open points on this line are the $T_{\rm g}$ determined from DSC. (b) Dielectric constant, $\varepsilon_{\rm s}$, vs inverse temperature. Dashed line for EO/Li = 10 is the fit to the Onsager relationship (eq 8).

which the VFT-fit of $\tau_{\alpha}=100$ s. The $T_{\rm g}$ values from DSC and DRS experiments are within 10 °C for both the EO/Li = 5 and EO/Li = 10 blends ($T_{\rm g\text{-}DSC}/T_{\rm g\text{-}DRS}$ is 19 °C/25 °C for EO/Li = 5, and -27 °C/-18 °C for EO/Li = 10); these magnitudes of difference are commonly reported for polymer electrolytes. This agreement in $T_{\rm g}$ suggests that the relaxation process in EO/Li = 5 and 10 is predominantly segmental relaxation and thus is labeled as the α process, noting that ion rearrangement will also be involved in the relaxation. In contrast, both the neat pSPhTFSI–Li and EO/Li = 2 blend exhibit Arrhenius behavior well before the relaxation time reaches 100 s, indicating that these relaxations are primarily not a result of segmental relaxation, but rather due to a rearrangement of ions and thus we have identified it as the α_2 process.

The dielectric constants, ε_s , of the ionomer and blends are shown in Figure 8b. In the blend of EO/Li = 10, the high dielectric constant results from strong dissociation of ions in the blend. Dielectric constants of similar magnitude have been previously seen in polyether–ester–sulfonate copolymer ionomers and are due to ion rearrangement associated with segmental relaxation. ^{57,60} The dielectric constant of EO/Li = 10 is fit to the Onsager equation ^{50,61,62}

$$\left(\frac{(\varepsilon_{\rm s} - \varepsilon_{\infty})(2\varepsilon_{\rm s} + \varepsilon_{\infty})}{\varepsilon_{\rm s}(\varepsilon_{\infty} + 2)^2}\right) = \frac{\nu_{\rm pair} m_{\rm pair}^2}{9\varepsilon_0 kT} \tag{8}$$

where $v_{\rm pair}$ and $m_{\rm pair}$ are the number and strength of ionic dipoles and $v_{\rm pair}m_{\rm pair}^2$ is the only fitting parameter, which is assumed to be temperature-independent. Below 100 °C, $\varepsilon_{\rm s}$ exhibits an excellent fit to eq 8, indicating that the EO/Li = 10 blend ($T_{\rm g}=-27$ °C) behaves as a simple polar liquid, which is common in ionomers above $T_{\rm g}^{-50,61,62}$ At temperatures >100 °C, the EO/Li = 10 blend diverges from this behavior, with a significant reduction in $\varepsilon_{\rm s}$. In previously studied ionomers, this divergence from the Onsager fit at high temperatures was a result of ion aggregation that leads to a loss in the dielectric constant. So,62 While the X-ray scattering of p5PhTFSI—Li does not suggest a structural transformation, the drop off of $d_{\rm i}$ above 90 °C (Figure 5) correlates with the reduction in the dielectric constant at high temperatures.

In contrast to EO/Li = 10, ε_s increases with temperature in the EO/Li = 0, 2, and 5 blends. While uncommon in ionomers, this has been previously reported in polymerized ionic liquids. This behavior is likely a result of the inverse

Haven ratio, where more ions are contributing to conductivity at higher temperature, giving a larger relaxation strength associated with the rearrangement of ions. The inverse Haven ratio has been reported in polymers that exhibit interconnected aggregates, which is consistent with the percolated aggregates based on our X-ray scattering results (Figure 3). A higher ε_s in EO/Li = 5 than EO/Li = 0 or 2 is likely due to aggregates swollen by PEO and thus greater ion rearrangement. Interestingly, ε_s is slightly higher in EO/Li = 0 than EO/Li = 2, even though EO/Li = 0 has no PEO and likely has a more tightly packed assembly. While ε_s is reduced with aggregation, the low dielectric constant of PEO may also reduce the overall ε_s of EO/Li = 2 relative to the neat p5PhTFSI–Li.

To gain further insight into the correlation between segmental relaxation and ion transport in EO/Li = 5 and EO/Li = 10, we construct a Walden plot. This is a double-logarithmic plot of the molar conductivity, Λ , versus the PEO relaxation time, τ_{ω} where ideal Walden behavior indicates strong coupling of ion transport to segmental motion, Figure 9. ^{12,15,16} The Walden behavior line is based on the ion conductivity of a dilute aqueous solution, with a slope of 1. The EO/Li = 5 blend exhibits Walden behavior similar to

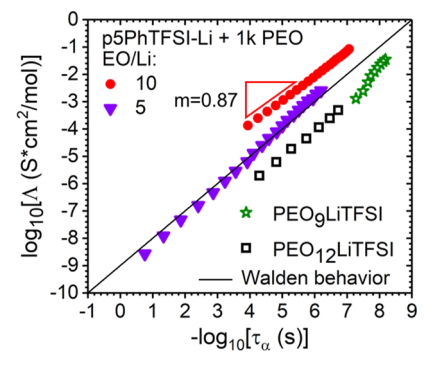


Figure 9. Λ vs τ_{α} of EO/Li = 5 and 10 blends (from 40 to 140 °C and 30 to 130 °C, respectively). The solid line is the ideal Walden line based on a dilute salt in water. 12,58,63 Λ was calculated using the VDW volume. 43 PEO₉LiTFSI data (from 25 to 65 °C) is included for reference and determined from conductivity and relaxation time values from Bandara et al. 64 PEO₁₂LiTFSI (from -35 to -5 °C) data is included for reference and determined from conductivity and relaxation time values from Das et al. 65

many other polymers and liquid electrolytes. However, EO/Li = 10 falls approximately 1 order of magnitude above the Walden line. This, combined with a slope of less than 1, suggests superionic transport, in which ion mobility is at least partially decoupled from the polymer.

Such superionic behavior has been previously reported in some Li-salt polymer electrolytes, as well as single-anion conducting polymers in the glassy state. 12,17,63 We believe Figure 9 is the first report of superionic transport in a singlelithium ion conductor above the $T_{\rm g}$. To better understand what is causing this superionic transport, it is critical to identify the mechanisms involved with ion mobility. In systems containing a Li-salt and PEO-based polymers, the Li⁺ ions coordinate to the ether oxygens, and ion mobility is coupled to the segmental motion of the polymer backbone. However, in SICs, the Li⁺ ions will typically move with the covalently bound anion or hop between neighboring anionic groups. Blending p5PhTFSI-Li with PEO leads to a competition between these transport mechanisms, and the resulting ion transport can vary depending on the amount of PEO, as evident by the "ideal" and "superionic" behavior in the EO/Li = 5 and EO/Li = 10 blends, respectively.

The superionic transport in the EO/Li = 10 blend suggests there is at least some decoupling of the ion conductivity from PEO segmental motion. A possible reason for this may be an increased ability of the Li⁺ ions to hop between TFSI⁻ anions due to PEO solvation. In a recent study of PEO with LiTFSI salt, a much higher fraction of free Li+ ions was reported for EO/Li = 10, compared to more negatively charged clusters with EO/Li = 5.70.66 At modest amounts of PEO, the PEO-TFSI complexes may disrupt the ability for PEO to fully solvate the Li+, thus promoting the hopping mechanism. At higher levels of PEO, such as our p5PhTFSI-Li EO/Li = 10 blend, there appears to be sufficient PEO to both fully solvate the Li⁺ ions and coordinate with the TFSI pendant groups. Consequently, the Li⁺ transport can be decoupled from the PEO dynamics, because the energy barrier for hopping is reduced. While the decoupling of Li⁺ conductivity from the backbone mobility in the EO/Li = 10 blend is promising, the balance between the TFSI⁻/Li⁺ and PEO/Li⁺ coordination strengths and the role of these interactions require further experiments and atomistic MD simulations.

In Figure 9, we also compare the molar conductivity of the p5PhTFSI-Li blends to that of LiTFSI salt in high-molecularweight PEO with similar PEO ratios: EO/Li = 9 and PEO $5,000,000 \text{ g mol}^{-1}$; ⁶⁴ EO/Li = 12 and PEO 400,000 g mol⁻¹.65 We note that both of these systems were studied above their T_o , and the EO/Li = 9 system was reported to be completely amorphous, while the EO/Li = 12 system was semicrystalline (~18% crystalline). Both PEO₉LiTFSI and PEO₁₂LiTFSI exhibit subionic behavior, where LiTFSI transport occurs even more slowly than segmental dynamics. The temperature ranges studied in PEO₉LiTFSI and PEO₁₂LiTFSI were much lower than in p5PhTFSI-Li EO/Li = 10 because the dynamics of PEO in the PEO-LiTFSI electrolytes are significantly faster than in our single-ion conducting system. For example, at 60 °C, $\tau_{\alpha} = 8 \times 10^{-9}$ s in PEO₉LiTFSI, compared to 3.6×10^{-6} s in p5PhTFSI-Li EO/Li = 10, a difference of nearly three orders of magnitude. However, the difference in conductivity at 60 °C is only about 1 order of magnitude (9 \times 10⁻⁵ S cm⁻¹ in PEO₉LiTFSI and 5.5×10^{-6} S cm⁻¹ in p5PhTFSI–Li EO/ Li = 10). This is consistent with the significant improvement toward superionic behavior in the p5PhTFSI-Li EO/Li = 10

blend. Note that a Li⁺ transference number of 1 was reported in the parallel study of p5PhTFSI–Li with 20,000 g mol⁻¹ PEO.³³ This result combined with the superionic transport reported here for a p5PhTFSI–Li/PEO blend with 1000 g mol⁻¹ PEO indicate the potential of SICs to achieve decoupled transport and high conductivity. While ion solvation was accomplished with low-molecular-weight PEO here, alternative solvation strategies can also be pursued in conjunction with SICs.

CONCLUSIONS

Polymer electrolyte blends were created with varying quantities of a low-molecular-weight PEO with p5PhTFSI–Li, a new precise SIC synthesized by a scalable ring-opening polymerization. We used a combination of experimental techniques to characterize the nanoscale morphology, ion transport, and segmental dynamics of these polymer electrolyte systems. These p5PhTFSI–Li and PEO blends are miscible in ratios up to at least EO/Li = 10, and are fully amorphous. While the ions form percolated assemblies that are nanophase separated from the backbone in neat p5PhTFSI–Li, the addition of PEO swells these polar aggregates and introduces interactions between the ions (Li⁺ and TFSI⁻) and PEO. At EO/Li = 5 and 10, the spacing between the TFSI⁻ anions is \sim 6 Å, which may facilitate ion transport.

The addition of 1000 g mol⁻¹ PEO results in a significant increase in conductivity relative to the neat p5PhTFSI–Li (over 7 orders of magnitude at 130 °C). The EO/Li = 10 blend has a conductivity of $\sigma_{\rm DC}$ of 3.8 × 10⁻⁵ S cm⁻¹ at 90 °C and 1.8 × 10⁻⁴ S cm⁻¹ at 130 °C, on par with other PEO-based single Li-ion conductors. From a Walden plot analysis of the conductivity and PEO relaxation time, we determined that the EO/Li = 10 blend exhibits some decoupled ion transport at $T \gg T_g$ which has not previously been reported in a single-Li ion conducting polymer melt. This behavior is likely a result of balancing the solvating action of PEO with both the covalently bound TFSI⁻ and Li⁺, such that the energy barrier for decoupled Li⁺ hopping is significantly reduced. These results suggest the value of solvating SICs to promote decoupled Li⁺ transport above the T_g .

Future work will explore additional ratios of EO/Li to determine an optimal blend composition that maximizes the degree of decoupling of Li⁺ from p5PhTFSI—Li and PEO. While this study has demonstrated a pathway to superionic transport, additional characterization of this or related systems is required to evaluate these materials as electrolytes for battery applications. This includes exploring the PEO molecular weight effects on the blend morphology and the ion transport mechanisms and probing the mechanical properties and electrochemical stability of these blends.

ASSOCIATED CONTENT

Solution Supporting Information

The Supporting Information is available free of charge at https://pubs.acs.org/doi/10.1021/acs.macromol.2c00459.

X-ray scattering fit; Nyquist plot fit; additional X-ray scattering data; reversibility and fitting parameters of conductivity; and fitting parameters of relaxation time (PDF)

AUTHOR INFORMATION

Corresponding Author

Karen I. Winey — Department of Materials Science & Engineering, University of Pennsylvania, Philadelphia, Pennsylvania 19104, United States; oorcid.org/0000-0001-5856-3410; Email: winey@seas.upenn.edu

Authors

- Benjamin A. Paren Department of Materials Science & Engineering, University of Pennsylvania, Philadelphia, Pennsylvania 19104, United States; Present Address: Massachusetts Institute of Technology, Research Laboratory of Electronics, 50 Vassar Street, Cambridge, MA, USA 02139; orcid.org/0000-0002-4361-5182
- Nam Nguyen Department of Chemistry and Biochemistry, Florida State University, Tallahassee, Florida 32306, United States
- Valerie Ballance Department of Materials Science & Engineering, University of Pennsylvania, Philadelphia, Pennsylvania 19104, United States
- Daniel T. Hallinan Department of Chemical and Biomedical Engineering, Florida A&M University—Florida State University (FAMU-FSU) College of Engineering, Tallahassee, Florida 32310, United States; orcid.org/ 0000-0002-3819-0992
- Justin G. Kennemur Department of Chemistry and Biochemistry, Florida State University, Tallahassee, Florida 32306, United States; orcid.org/0000-0002-2322-0386

Complete contact information is available at: https://pubs.acs.org/10.1021/acs.macromol.2c00459

Author Contributions

The manuscript was written through contributions of all authors. All authors have given approval to the final version of the manuscript.

Funding

K.I.W. and B.A.P. acknowledge funding from the National Science Foundation (NSF) DMR 1904767 and NSF PIRE 1545884. J.G.K., N.N., and D.T.H. acknowledge funding from NSF 1804871.

Notes

The authors declare no competing financial interest.

REFERENCES

- (1) Armand, M.; Tarascon, J.-M. Building Better Batteries. *Nature* **2008**, 451, 652–657.
- (2) Morris, M. A.; An, H.; Lutkenhaus, J. L.; Epps, T. H. Harnessing the Power of Plastics: Nanostructured Polymer Systems in Lithium-Ion Batteries. *ACS Energy Lett.* **2017**, *2*, 1919–1936.
- (3) Blomgren, G. E. The Development and Future of Lithium Ion Batteries. J. Electrochem. Soc. 2017, 164, AS019-AS025.
- (4) Fenton, D. E.; Parker, M.; Wright, P.Complexes of alkali metal ions with poly(ethylene oxide)*Polymer***1973**14589
- (5) Wright, P. v. Electrical Conductivity in Ionic Complexes of Poly(Ethylene Oxide); Wiley, 1975; Vol. 7, pp 319-327.
- (6) Xue, Z.; He, D.; Xie, X. Poly(Ethylene Oxide)-Based Electrolytes for Lithium-Ion Batteries. J. Mater. Chem. A 2015, 3, 19218–19253.
- (7) Diederichsen, K. M.; McShane, E. J.; McCloskey, B. D. Promising Routes to a High Li+ Transference Number Electrolyte for Lithium Ion Batteries. *ACS Energy Lett.* **2017**, *2*, 2563–2575.
- (8) Young, W.-S.; Kuan, W.-F.; Epps, T. H. Block Copolymer Electrolytes for Rechargeable Lithium Batteries. *J. Polym. Sci., Part B: Polym. Phys.* **2014**, *52*, 1–16.

- (9) Blatt, M. P.; Hallinan, D. T. Polymer Blend Electrolytes for Batteries and Beyond. *Ind. Eng. Chem. Res.* **2021**, *60*, 17303–17327.
- (10) Liu, J.; Pickett, P. D.; Park, B.; Upadhyay, S. P.; Orski, S. V.; Schaefer, J. L. Non-Solvating, Side-Chain Polymer Electrolytes as Lithium Single-Ion Conductors: Synthesis and Ion Transport Characterization. *Polym. Chem.* **2020**, *11*, 461–471.
- (11) Stacy, E. W.; Gainaru, C. P.; Gobet, M.; Wojnarowska, Z.; Bocharova, V.; Greenbaum, S. G.; Sokolov, A. P. Fundamental Limitations of Ionic Conductivity in Polymerized Ionic Liquids. *Macromolecules* **2018**, *51*, 8637–8645.
- (12) Fan, F.; Wang, Y.; Hong, T.; Heres, M. F.; Saito, T.; Sokolov, A. P. Ion Conduction in Polymerized Ionic Liquids with Different Pendant Groups. *Macromolecules* **2015**, *48*, 4461–4470.
- (13) Noor, S. A. M.; Sun, J.; Macfarlane, D. R.; Armand, M.; Gunzelmann, D.; Forsyth, M. Decoupled Ion Conduction in Poly(2-Acrylamido-2-Methyl-1-Propane-Sulfonic Acid) Homopolymers. *J. Mater. Chem. A* **2014**, *2*, 17934–17943.
- (14) Mohd Noor, S. A.; Gunzelmann, D.; Sun, J.; MacFarlane, D. R.; Forsyth, M. Ion Conduction and Phase Morphology in Sulfonate Copolymer Ionomers Based on Ionic Liquid-Sodium Cation Mixtures. *J. Mater. Chem. A* **2014**, *2*, 365–374.
- (15) Bresser, D.; Lyonnard, S.; Iojoiu, C.; Picard, L.; Passerini, S. Decoupling Segmental Relaxation and Ionic Conductivity for Lithium-Ion Polymer Electrolytes. *Molecular Systems Design and Engineering*; Royal Society of Chemistry, 2019; Vol. 4, pp 779–792.
- (16) Wang, Y.; Fan, F.; Agapov, A. L.; Yu, X.; Hong, K.; Mays, J.; Sokolov, A. P. Design of Superionic Polymers New Insights from Walden Plot Analysis. *Solid State Ionics* **2014**, *262*, 782–784.
- (17) Angell, C. A.; Liu, C.; Sanchez, E. Rubbery Solid Electrolytes with Dominant Cationic Transport and High Ambient Conductivity. *Nature* **1993**, 362, 137–139.
- (18) Jones, S. D.; Nguyen, H.; Richardson, P. M.; Chen, Y.-Q.; Wyckoff, K. E.; Hawker, C. J.; Clément, R. J.; Fredrickson, G. H.; Segalman, R. A. Design of Polymeric Zwitterionic Solid Electrolytes with Superionic Lithium Transport. ACS Cent. Sci. 2022, 8, 169–175.
- (19) Paren, B. A.; Thurston, B. A.; Neary, W. J.; Kendrick, A.; Kennemur, J. G.; Stevens, M. J.; Frischknecht, A. L.; Winey, K. I. Percolated Ionic Aggregate Morphologies and Decoupled Ion Transport in Precise Sulfonated Polymers Synthesized by Ring-Opening Metathesis Polymerization. *Macromolecules* **2020**, *53*, 8960–8973.
- (20) Frischknecht, A. L.; Paren, B. A.; Middleton, L. R.; Koski, J. P.; Tarver, J. D.; Tyagi, M.; Soles, C. L.; Winey, K. I. Chain and Ion Dynamics in Precise Polyethylene Ionomers. *Macromolecules* **2019**, 52, 7939–7950.
- (21) Lin, K.-J.; Maranas, J. K. Superionic Behavior in Polyethylene-Oxide-Based Single-Ion Conductors. *Phys. Rev. E: Stat., Nonlinear, Soft Matter Phys.* **2013**, 88, 1–5.
- (22) Kisliuk, A.; Bocharova, V.; Popov, I.; Gainaru, C.; Sokolov, A. P. Fundamental Parameters Governing Ion Conductivity in Polymer Electrolytes. *Electrochim. Acta* **2019**, 299, 191–196.
- (23) Kendrick, A.; Neary, W. J.; Delgado, J. D.; Bohlmann, M.; Kennemur, J. G. Precision Polyelectrolytes with Phenylsulfonic Acid Branches at Every Five Carbons. *Macromol. Rapid Commun.* **2018**, *39*, 1800145.
- (24) Neary, W. J.; Kennemur, J. G. A Precision Ethylene-Styrene Copolymer with High Styrene Content from Ring-Opening Metathesis Polymerization of 4-Phenylcyclopentene. *Macromol. Rapid Commun.* **2016**, *37*, 975–979.
- (25) Cheng, Y.; Yang, J.; Hung, J.-H.; Patra, T. K.; Simmons, D. S. Design Rules for Highly Conductive Polymeric Ionic Liquids from Molecular Dynamics Simulations. *Macromolecules* **2018**, *51*, 6630–6644.
- (26) Zhao, Y.; Tao, R.; Fujinami, T. Enhancement of Ionic Conductivity of PEO-LiTFSI Electrolyte upon Incorporation of Plasticizing Lithium Borate. *Electrochim. Acta* **2006**, *S1*, 6451–6455. (27) Brooks, D. J.; Merinov, B. v.; Goddard, W. A.; Kozinsky, B.;

Mailoa, J. Atomistic Description of Ionic Diffusion in PEO-LiTFSI:

- Effect of Temperature, Molecular Weight, and Ionic Concentration. *Macromolecules* **2018**, *51*, 8987–8995.
- (28) Loo, W. S.; Mongcopa, K. I.; Gribble, D. A.; Faraone, A. A.; Balsara, N. P. Investigating the Effect of Added Salt on the Chain Dimensions of Poly(Ethylene Oxide) through Small-Angle Neutron Scattering. *Macromolecules* **2019**, *52*, 8724–8732.
- (29) Meziane, R.; Bonnet, J.-P.; Courty, M.; Djellab, K.; Armand, M. Single-Ion Polymer Electrolytes Based on a Delocalized Polyanion for Lithium Batteries. *Electrochim. Acta* **2011**, *57*, 14–19.
- (30) Bouchet, R.; Maria, S.; Meziane, R.; Aboulaich, A.; Lienafa, L.; Bonnet, J.-P.; Phan, T. N. T.; Bertin, D.; Gigmes, D.; Devaux, D.; Denoyel, R.; Armand, M. Single-Ion BAB Triblock Copolymers as Highly Efficient Electrolytes for Lithium-Metal Batteries. *Nat. Mater.* **2013**, *12*, 452–457.
- (31) Piszcz, M.; Garcia-Calvo, O.; Oteo, U.; Lopez del Amo, J. M.; Li, C.; Rodriguez-Martinez, L. M.; Youcef, H. B.; Lago, N.; Thielen, J.; Armand, M. New Single Ion Conducting Blend Based on PEO and PA-LiTFSI. *Electrochim. Acta* **2017**, *255*, 48–54.
- (32) Porcarelli, L.; Aboudzadeh, M. A.; Rubatat, L.; Nair, J. R.; Shaplov, A. S.; Gerbaldi, C.; Mecerreyes, D. Single-Ion Triblock Copolymer Electrolytes Based on Poly(Ethylene Oxide) and Methacrylic Sulfonamide Blocks for Lithium Metal Batteries. *J. Power Sources* **2017**, 364, 191–199.
- (33) Nguyen, N.; Blatt, P. M.; Kim, K.; Hallinan, D. T.; Kennemur, J. G. Investigating Miscibility and Lithium Ion Transport in Blends of Poly(ethylene oxide) with a Polyanion Containing Precisely-Spaced Delocalized Charges. Sumbitted.
- (34) Pielichowski, K.; Flejtuch, K. Differential Scanning Calorimetry Studies on Poly(Ethylene Glycol) with Different Molecular Weights for Thermal Energy Storage Materials. *Polym. Adv. Technol.* **2003**, *13*, 690–696
- (35) Cao, P.-F.; Wojnarowska, Z.; Hong, T.; Carroll, B.; Li, B.; Feng, H.; Parsons, L.; Wang, W.; Lokitz, B. S.; Cheng, S.; Bocharova, V.; Sokolov, A. P.; Saito, T. A Star-Shaped Single Lithium-Ion Conducting Copolymer by Grafting a POSS Nanoparticle. *Polymer (Guildf)* 2017, 124, 117–127.
- (36) Qiu, Z.; Ikehara, T.; Nishi, T. Miscibility and Crystallization in Crystalline/Crystalline Blends of Poly(Butylene Succinate)/Poly(Ethylene Oxide). *Polymer (Guildf)* **2003**, *44*, 2799–2806.
- (37) Kim, H. J.; Peng, X.; Shin, Y.; Hillmyer, M. A.; Ellison, C. J. Blend Miscibility of Poly(Ethylene Terephthalate) and Aromatic Polyesters from Salicylic Acid. *J. Phys. Chem. B* **2021**, 125, 450–460.
- (38) Gordon, M.; Taylor, J. S. Ideal Copolymers and the Second-Order Transitions of Synthetic Rubbers. i. Non-Crystalline Copolymers. *J. Appl. Chem.* **1952**, *2*, 493–500.
- (39) Choi, U. H.; Liang, S.; O'Reilly, M. v.; Winey, K. I.; Runt, J.; Colby, R. H. Influence of Solvating Plasticizer on Ion Conduction of Polysiloxane Single-Ion Conductors. *Macromolecules* **2014**, *47*, 3145–3153.
- (40) Olmedo-Martínez, J. L.; Porcarelli, L.; Alegría, Á.; Mecerreyes, D.; Müller, A. J.; Mecerreyes, D.; Müller, A. J. High Lithium Conductivity of Miscible Poly(Ethylene Oxide)/Methacrylic Sulfonamide Anionic Polyelectrolyte Polymer Blends. *Macromolecules* **2020**, *53*, 4442–4453.
- (41) O'Reilly, M. v.; Masser, H.; King, D. R.; Painter, P. C.; Colby, R. H.; Winey, K. I.; Runt, J. Ionic Aggregate Dissolution and Conduction in a Plasticized Single-Ion Polymer Conductor. *Polymer (Guildf)* **2015**, *59*, 133–143.
- (42) Zhang, Z.; Liu, C.; Cao, X.; Wang, J.-H. H.; Chen, Q.; Colby, R. H. Morphological Evolution of Ionomer/Plasticizer Mixtures during a Transition from Ionomer to Polyelectrolyte. *Macromolecules* **2017**, *50*, 963–971.
- (43) Zhao, Y. H.; Abraham, M. H.; Zissimos, A. M. Fast Calculation of van Der Waals Volume as a Sum of Atomic and Bond Contributions and Its Application to Drug Compounds. *J. Org. Chem.* **2003**, *68*, 7368–7373.
- (44) Sorte, E. G.; Paren, B. A.; Rodriguez, C. G.; Fujimoto, C.; Poirier, C.; Abbott, L. J.; Lynd, N. A.; Winey, K. I.; Frischknecht, A. L.; Alam, T. M.; Rodriguez, C. G.; Fujimoto, C.; Poirier, C.; Abbott,

- L. J.; Lynd, N. A.; Winey, K. I.; Frischknecht, A. L.; Alam, T. M. Impact of Hydration and Sulfonation on the Morphology and Ionic Conductivity of Sulfonated Poly(Phenylene) Proton Exchange Membranes. *Macromolecules* **2019**, *52*, 857–876.
- (45) Paren, B. A.; Thurston, B. A.; Kanthawar, A.; Neary, W. J.; Kendrick, A.; Maréchal, M.; Kennemur, J. G.; Stevens, M. J.; Frischknecht, A. L.; Winey, K. I. Fluorine-Free Precise Polymer Electrolyte for Efficient Proton Transport: Experiments and Simulations. *Chem. Mater.* **2021**, 33, 6041–6051.
- (46) Paren, B. A.; Raghunathan, R.; Knudson, I. J.; Freyer, J. L.; Campos, L. M.; Winey, K. I. Impact of Building Block Structure on Ion Transport in Cyclopropenium-Based Polymerized Ionic Liquids. *Polym. Chem.* **2019**, *10*, 2832–2839.
- (47) Choi, U. H.; Ye, Y.; Salas de la Cruz, D.; Liu, W.; Winey, K. I.; Elabd, Y. A.; Runt, J.; Colby, R. H. Dielectric and Viscoelastic Responses of Imidazolium-Based Ionomers with Different Counterions and Side Chain Lengths. *Macromolecules* **2014**, 47, 777–790.
- (48) Liu, H.; Paddison, S. J. Direct Comparison of Atomistic Molecular Dynamics Simulations and X-Ray Scattering of Polymerized Ionic Liquids. *ACS Macro Lett.* **2016**, *5*, 537–543.
- (49) Loo, W. S.; Fang, C.; Balsara, N. P.; Wang, R. Uncovering Local Correlations in Polymer Electrolytes by X-Ray Scattering and Molecular Dynamics Simulations. *Macromolecules* **2021**, *54*, 6639–6648
- (50) Wang, W.; Tudryn, G. J.; Colby, R. H.; Winey, K. I. Thermally Driven Ionic Aggregation in Poly(Ethylene Oxide)-Based Sulfonate Ionomers. *J. Am. Chem. Soc.* **2011**, *133*, 10826–10831.
- (51) Ma, Q.; Xia, Y.; Feng, W.; Nie, J.; Hu, Y.-S.; Li, H.; Huang, X.; Chen, L.; Armand, M.; Zhou, Z. Impact of the Functional Group in the Polyanion of Single Lithium-Ion Conducting Polymer Electrolytes on the Stability of Lithium Metal Electrodes. *RSC Adv.* **2016**, *6*, 32454–32461.
- (52) Kremer, F.; Schönhals, A. Broadband Dielectric Spectroscopy; Springer-Verlag: Berlin, 2002.
- (53) di Noto, V.; Vittadello, M.; Yoshida, K.; Lavina, S.; Negro, E.; Furukawa, T. Broadband Dielectric and Conductivity Spectroscopy of Li-Ion Conducting Three-Dimensional Hybrid Inorganic-Organic Networks as Polymer Electrolytes Based on Poly(Ethylene Glycol) 400, Zr and Al Nodes. *Electrochim. Acta* 2011, 57, 192–200.
- (54) di Noto, V.; Gliubizzi, R.; Negro, E.; Pace, G. Effect of SiO2 on Relaxation Phenomena and Mechanism of Ion Conductivity of [Nafion/(SiO2)x] Composite Membranes. *J. Phys. Chem. B* **2006**, 110, 24972–24986.
- (55) di Noto, V.; Negro, E.; Sanchez, J.-Y.; Iojoiu, C. Structure-Relaxation Interplay of a New Nanostructured Membrane Based on Tetraethylammonium Trifluoromethanesulfonate Ionic Liquid and Neutralized Nafion 117 for High-Temperature Fuel Cells. *J. Am. Chem. Soc.* **2010**, *132*, 2183–2195.
- (56) Choi, U. H.; Price, T. L.; Schoonover, D. v.; Gibson, H. W.; Colby, R. H. The Effect of Oligo(Oxyethylene) Moieties on Ion Conduction and Dielectric Properties of Norbornene-Based Imidazolium Tf2N Ionic Liquid Monomers. *Macromolecules* **2020**, *53*, 4990–5000.
- (57) Tudryn, G. J.; O'Reilly, M. V.; Dou, S.; King, D. R.; Winey, K. I.; Runt, J.; Colby, R. H. Molecular Mobility and Cation Conduction in Polyether-Ester-Sulfonate Copolymer Ionomers. *Macromolecules* **2012**, *45*, 3962–3973.
- (58) Fan, F.; Wang, Y.; Sokolov, A. P. Ionic Transport, Microphase Separation, and Polymer Relaxation in Poly(Propylene Glycol) and Lithium Perchlorate Mixtures. *Macromolecules* **2013**, *46*, 9380–9389.
- (59) Yoshida, K.; Manabe, H.; Takahashi, Y.; Furukawa, T. Correlation between Ionic and Molecular Dynamics in the Liquid State of Polyethylene Oxide/Lithium Perchlorate Complexes. *Electrochim. Acta* **2011**, *57*, 139–146.
- (60) Fragiadakis, D.; Dou, S.; Colby, R. H.; Runt, J. Molecular Mobility and Li+ Conduction in Polyester Copolymer Ionomers Based on Poly(Ethylene Oxide). *J. Chem. Phys.* **2009**, *130*, 063659.
- (61) Onsager, L. Electric Moments of Molecules in Liquids. J. Am. Chem. Soc. 1936, 58, 1486.

- (62) Choi, U. H.; Lee, M.; Wang, S.; Liu, W.; Winey, K. I.; Gibson, H. W.; Colby, R. H. Ionic Conduction and Dielectric Response of Poly(Imidazolium Acrylate) Ionomers. *Macromolecules* **2012**, *45*, 3974–3985.
- (63) Wang, Y.; Fan, F.; Agapov, A. L.; Saito, T.; Yang, J.; Yu, X.; Hong, K.; Mays, J.; Sokolov, A. P. Examination of the Fundamental Relation between Ionic Transport and Segmental Relaxation in Polymer Electrolytes. *Polymer (Guildf)* **2014**, *55*, 4067–4076.
- (64) Bandara, L. R. A. K.; Dissanayake, M. A. K. L.; Furlani, M.; Mellander, B.-E. Broad Band Dielectric Behaviour of Plasticized PEO-Based Solid Polymer Electrolytes. *Ionics* **2000**, *6*, 239–247.
- (65) Das, S.; Ghosh, A. Ion Conduction and Relaxation in PEO-LiTFSI-Al2O3 Polymer Nanocomposite Electrolytes. *J. Appl. Phys.* **2015**, *117*, 174103.
- (66) Popovic, J. Dry Polymer Electrolyte Concepts for Solid-state Batteries. *Macromol. Chem. Phys.* **2021**, 223, 2100344.

TRECOMMENDED Recommended by ACS

Extrusion of Polymer Blend Electrolytes for Solid-State Lithium Batteries: A Study of Polar Functional Groups

Léa Caradant, Mickaël Dollé, et al.

NOVEMBER 12, 2021

ACS APPLIED POLYMER MATERIALS

READ 🗹

Ion-Conducting Dynamic Solid Polymer Electrolyte Adhesives

Ryo Kato, Stuart J. Rowan, et al.

MARCH 19, 2020

ACS MACRO LETTERS

READ 🗹

Modifying Li+ and Anion Diffusivities in Polyacetal Electrolytes: A Pulsed-Field-Gradient NMR Study of Ion Self-Diffusion

David M. Halat, Jeffrey A. Reimer, et al.

JUNE 29, 2021

CHEMISTRY OF MATERIALS

READ 🗹

Ion Conductivity-Shear Modulus Relationship of Single-Ion Solid Polymer Electrolytes Composed of Polyanionic Miktoarm Star Copolymers

Georgia Nikolakakou, Emmanouil Glynos, et al.

JULY 05, 2022

MACROMOLECULES

READ 🗹

Get More Suggestions >